JACS
JOURNAL OF THE AMERICAN CHEMICAL SOCIETY
Article
pubs.acs.org/JACS

On the pH-Dependent Quenching of Quantum Dot Photoluminescence by Redox Active Dopamine

Xin Ji, Goutam Palui, Tommaso Avellini,† Hyon Bin Na, Chongyue Yi, Kenneth L. Knappenberger, Jr., and Hedi Mattoussi*

Department of Chemistry and Biochemistry, Florida State University, Tallahassee, Florida 32306, United States

Supporting Information

ABSTRACT: We investigated the charge transfer interactions between luminescent quantum dots (QDs) and redox active dopamine. For this, we used pH-insensitive ZnS-overcoated CdSe QDs rendered water-compatible using poly (ethylene glycol)-appended dihydrolipoic acid (DHLA-PEG), where a fraction of the ligands was amine-terminated to allow for controlled coupling of dopamine−isothiocyanate onto the nanocrystal. Using this sample configuration, we probed the effects of changing the density of dopamine and the buffer pH on the fluorescence properties of these conjugates. Using steady-state and time-resolved fluorescence, we measured a pronounced pH-dependent photoluminescence (PL) quenching for all QD-dopamine assemblies. Several parameters affect the PL loss. First, the quenching efficiency strongly depends on the number of dopamines per QD-conjugate. Second, the quenching efficiency is substantially increased in alkaline buffers. Third, this pH-dependent PL loss can be completely eliminated when oxygen-depleted buffers are used, indicating that oxygen plays a crucial role in the redox activity of dopamine. We attribute these findings to charge transfer interactions between QDs and mainly two forms of dopamine: the reduced catechol and oxidized quinone. As the pH of the dispersions is changed from acidic to basic, oxygen-catalyzed transformation progressively reduces the dopamine potential for oxidation and shifts the equilibrium toward increased concentration of quinones. Thus, in a conjugate, a QD can simultaneously interact with quinones (electron acceptors) and catechols (electron donors), producing pH-dependent PL quenching combined with shortening of the exciton lifetime. This also alters the recombination kinetics of the electron and hole of photoexcited QDs. Transient absorption measurements that probed intraband transitions supported those findings where a simultaneous pronounced change in the electron and hole relaxation rates was measured when the pH was changed from acidic to alkaline.

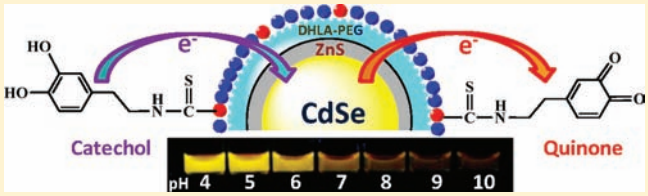

INTRODUCTION

Colloidal semiconductor nanocrystals and nanorods (quantum dots and quantum rods, QDs and QRs, respectively) combine several unique optical and spectroscopic properties, which can be tuned via size and/or composition.[1−8] Core−shell QDs, such as those made of ZnS-overcoated nanocrystals, exhibit narrow tunable emission with high quantum yields and a pronounced photo and chemical stability.[5,9−12] They can also be surface-functionalized with a variety of bifunctional molecules, which allow their dispersion in, and processing from, solution media.[13−23] Since the mid 1990s, various groups have proposed and tested QDs as fluorescent platforms for sensing and imaging in biology.[24−28] Because of the presence of a large fraction of their atoms on their surfaces, the QD photoemission as well as other properties can be strongly affected by the nature of the capping ligands,[29−32] the surrounding matrix,[17,33,34] and by proximal fluorescent dyes and metal/redox complexes.[35−41] These changes can be induced by nonradiative transfer of excitation to proximal dyes (in case of Förster resonance energy transfer),[36,38,42] or by charge transfer interactions when metal complexes are brought in close proximity to the QD surfaces.[35,37,40,43]

Dopamine is a natural compound with critical biological functions involving brain activity and neurotransmission.[44−46] It is involved in many brain functions and behaviors, such as cognition, motivation, sleep, attention, and learning. Dopamine and some of its derivatives exhibit complex redox properties with pH-tunable oxidation and reduction potentials.[47] Its pH-dependent properties have made it a more complex yet attractive system to probe and understand. Interactions of dopamine (and dopamine derivatives) with luminescent QDs have been explored by several groups in the past few years, due to the richness of such system and the potentials it offers for developing sensing assemblies.[48−54] In one example, Nadeau and co-workers reported that CdSe QDs attached to dopamine could stain cells that express dopamine-receptors in redox-sensitive patterns; they found that the environment around the QD-conjugates could influence their fluorescence.[49,54] They attributed the results to electron transfer between dopamine and QDs. They also proposed that toxicity to cells induced by singlet oxygen generation in the presence of photoexcited QDs could be reduced with the addition of reducing agents

Received: January 22, 2012
Published: March 6, 2012

   dx.doi.org/10.1021/ja300724x | J. Am. Chem. Soc. 2012, 134, 6006−6017

antioxidants at high concentrations.[49] In another example, Willner and co-workers used QD-peptide-tyrosine conjugates to probe tyrosinase and thrombin activities in solution.[50] Oxidation of tyrosine (induced by tyrosinase in the presence of O_2) to quinone bound to the nanocrystal surfaces produced substantial quenching of the QD luminescence; such process was attributed to energy transfer between the QDs and proximal quinones. Addition of thrombin specifically cleaved the peptide substrate, resulting in recovery of the QD emission that depended on the enzyme concentration.[50] In a third example, Santra and co-workers used QD-dopamine conjugates as sensing platforms to detect the presence of glutathione (GSH) in solution.[51] In particular, they used dopamine-coupled thiol-appended ligands (carbon disulfide linker) to functionalize their QDs, which severely quenched their photoemission. They then probed the ability of added glutathione to displace the dopamine-ligands, resulting in the progressive and GSH-dependent recovery of the QD emission.

We have investigated the photoemission properties of QD-peptide-dopamine conjugates formed via metal-affinity driven self-assembly between dopamine-functionalized, hexa-histidine (His_6)-tagged peptides and Zn-overcoated CdSe QDs.[52] We measured dopamine-induced quenching of the QDs both in vitro and microinjected in live cells. We found that measurable quenching of the QD emission required rather large numbers of His-peptide-dopamine to be added to the QD dispersions. For example, molar ratios of peptide-dopamine varying from 20 to 40 were required to induce 40% loss in QD photoluminescence (QD PL).

Cumulatively, these studies indicate that quinones and especially dopamine can engage in redox active interactions with QDs, resulting in pH-dependent change in QD PL. However, a clear understanding of the mechanisms that drive such interactions has not been achieved yet. Furthermore, inconsistencies between results reported by different groups and using various QD-dopamine constructs continue to exist. Some of the inconsistencies can be traced to a lack of control over the QD and/or the QD-dopamine constructs used, combined with the vastly different conditions used to probe such interactions. Moreover, the QD materials employed in some of these studies utilized core only QDs and/or relied on surface functionalization strategies that do not always guarantee pH "inertness" and long-term colloidal stability; this has complicated data analysis and interpretation. Also, lack of control over the number of bound dopamine or use of potentially pH-sensitive coupling strategy (such as metal–histidine coordination) can affect data and interpretation.

In this report, we explored the effects of dopamine on the QD PL using a more controlled construct, where the dopamine groups are covalently attached at the end of the surface functionalizing ligands. For this ,we used QDs cap exchanged with a mixture of DHLA-PEG-OCH_3 and DHLA-PEG-NH_2 ligands, and varied the relative fraction of amine to methoxy groups; these bidentate PEGylated ligands provide QDs with a pH-independent emission over pH 4–12. This permitted us to controllably vary the number of dopamines per QD, while maintaining the average separation distance fixed. We explored the effects of tuning the number of dopamine groups, the pH, and investigated the importance of oxygen (O_2) on the optical and spectroscopic properties of the QD-dopamine conjugates. We measured pronounced rates of PL loss combined with substantial shortening of the QD exciton lifetime in the presence of dopamine complexes. The present quenching rates are much higher than what we measured for self-assembled QD-peptide-dopamine assemblies.[52] We also found that oxygen present in the atmosphere plays a crucial role in the redox properties of dopamine alone and in the measured changes of the fluorescence properties of QD-dopamine conjugates. Transient absorption measurements supported those findings where a simultaneous change in the electron and hole intraband relaxation rates was measured when the pH was changed from acidic to alkaline.

EXPERIMENTAL SECTION

Synthesis of Dopamine-Isothiocyanate (Dopamine-ITC). We followed the synthetic schemes described in refs 52,55–57. 3-Hydroxytyramine hydrochloride (1.5 g, 7.9 mmol) was partially dissolved in tetrahydrofuran (20 mL) containing triethylamine (1.2 mL, 8.6 mmol), and then methanol (18 mL) was slowly added to this solution with stirring; addition was carried out at room temperature. Carbon disulfide (2.42 mL, 40.2 mmol) was added dropwise under ice cold conditions, and the solution was left stirring for 2 h; a light yellow color developed.[55] The reaction mixture was then allowed to warm to room temperature while stirring for an additional ~10–12 h. The mixture was again cooled to 0–5 °C (using an ice bath), and 30% hydrogen peroxide solution (2.52 mL, 26.3 mmol) as dehydrosulfurization reagent was slowly added.[56] The mixture was neutralized with hydrochloric acid (2 mL) and then concentrated under vacuum. The residue was filtered and rinsed with DI water (10 mL, three times), and then the filtrate was extracted with ethyl acetate (4–5 times, ~30 mL each). The organic layers were combined, dried over Na_2SO_4, and filtered. The solvent was evaporated to obtain the crude product, which was chromatographed on a silica column (100–200 mesh) using chloroform/ethyl acetate (3:1) mixture, yielding the compound as yellow oil. ^{1}H NMR and chemical ionization mass spectra of the purified compound are provided in the Supporting Information.

Synthesis of Dopamine-Modified PEG-Methoxy (Dopamine-PEG-OCH_3). In a 50 mL round-bottom flask dopamine-ITC (200 mg, 1.02 mmol) was dispersed in a mixture of deionized water/dimethyl sulfoxide (95:5, 10 mL total). The temperature of the flask with the reaction mixture was cooled to ~0 °C (using an ice bath), and then 500 mg of NH_2-PEG_{750}-methoxy (0.66 mmol) was added and the mixture was left stirring under nitrogen atmosphere overnight (~10–12 h). The solution was extracted with chloroform (4–5 times, 25 mL each), and the organic layers were combined, dried over Na_2SO_4, and filtered using a paper filter. The solvent was removed using a rotary evaporator, yielding the crude product, which was further purified by liquid chromatography on a silica gel column using chloroform/methanol (97:3) mixture for elution, to yield the pure compound as yellowish oil. ^{1}H NMR analysis confirmed the presence of the catechol moieties (with a multiplet peak at δ 6.59–6.80 ppm), the PEG moieties (pronounced peaks at δ 3.56–3.66 ppm), along with the methoxy groups (a sharp peak at δ 3.38 ppm) in the final product; spectra are provided in the Supporting Information.

Assembly of the QD-Dopamine Conjugates. We used a set of ZnS-overcoated CdSe QDs emitting at 572 nm. The nanocrystals were grown using a stepwise reaction involving the reduction of organometallic precursors at high temperature and in a coordinating solvent mixture made of trioctyl phosphine (TOP), trioctyl phosphine oxide (TOPO), and alkylamines. Core growth was then followed by overcoating with ZnS; additional details can be found in previous references.[1,4,5,9–12,58,59] The hydrophilic QDs were prepared via cap exchange with mixed ligands, methoxy-terminated DHLA-PEG_{750} and amine-terminated DHLA-PEG_{600}. These ligands were synthesized and purified using procedures described in previous publications.[13,19,60] The desired molar fraction of DHLA-PEG-NH_2 was added to DHLA-PEG-OCH_3, and the mixture was used for cap exchange. Here, the mixed ligands scheme allows the introduction of a small but controlled fraction of terminal amines on the nanocrystal surface.[60,61] These QDs were then reacted with the dopamine-ITC to provide the final QD-dopamine conjugates. Briefly, to a vial containing 1 mL of DI water we added 100 μL of amine-functionalized QDs (QD concentrations ~7–

dx.doi.org/10.1021/ja300724x | J. Am. Chem. Soc. 2012, 134, 6006–6017

9 μM) and the desired molar amounts (10−100 μL, depending on the molar ratio needed) of dopamine-ITC predissolved in DMSO. Dopamine was added in excess; for example, a molar ratio ranging from 2:1 to 180:1 with respect to the QD concentration was used for 5% DHLA-PEG-NH_2-QDs. The mixture was stirred for 3−3.5 h in the dark, followed by removal of excess free/unreacted dopamine using 1 round of concentration/dilution through a membrane filtration device (M_w cutoff: 50 kDa, Millipore). Aliquots (40 μL) of the QD-conjugate (stock) dispersions were then mixed with 960 μL of phosphate buffer (10 mM) at the desired pH before the florescence spectra were collected.

Conjugation under Argon Atmosphere. First, both DI water and 10 mM phosphate buffer solutions were degassed by bubbling argon for 3−3.5 h while stirring. Next, 1 mL of this degassed water was added to 100 μL of the desired amine-functionalized QDs in a sealed vial. Argon gas was further bubbled through the solutions, followed by addition of the required amount of dopamine-ITC predispersed in DMSO; the coupling reactions were allowed to proceed for ∼3.5 h. The QD-dopamine conjugates were then purified from free unreacted dopamine-ITC via 1 round of concentration/dilution using a membrane filtration device (as described above) and argon-saturated DI water. Argon was further bubbled through the purified conjugate dispersions for another 30 min before UV−vis, and fluorescence data were collected to remove any residual oxygen introduced by the filtration device.

Cyclic Voltammetry Measurements. Cyclic voltammograms (CV) were recorded on a CH Instruments 600D electrochemical analyzer at the sweep rate of 0.01 V s^{-1}. A platinum (Pt) working electrode and Ag^+ (0.01 M $AgNO_3$)/Ag reference electrode were used. The buffers were adjusted as: H_3PO_4 and NaH_2PO_4 for pH 2−4; Na_2HPO_4 and NaH_2PO_4 for pH 5−9; and Na_3PO_4 and Na_2HPO_4 for pH 10−12. The solution was degassed with a blanket of N_2 for 5 min prior to data collection. CV spectra of the blank solutions containing only the electrolyte were collected first assuring that the background was clean. The final C−V curves of the dopamine-PEG-OCH_3 solutions (at each pH) were reported after subtracting the background contribution (buffer only control); attaching the dopamine onto a PEG segment promotes easy dispersion in buffers.

Instrumentation, Fluorescence Measurements, and Data Analysis. Solvent evaporation was carried using a lab-scale Buchi rotary evaporator R-215 (New Castle, DE). ^{1}H NMR spectra were recorded using 600 MHz spectrometer (Bruker SpectroSpin 600 MHz). The optical absorption measurements were carried out using a UV−vis absorption spectrophotometer (UV 2450 model from Shimadzu), while a Fluorolog-3 spectrometer (HORIBA Jobin Yvon Inc., Edison, NJ), equipped with a TBX PMT detector and an air cooled CCD camera, was used to collect the steady-state fluorescence spectra. The time-resolved (TR) fluorescence decays were collected and analyzed using a TCSPC (time correlation single photon counting) system mounted on the same Fluorolog-3 above. We used a pulsed excitation signal at 440 nm and a repetition rate of 1 MHz, provided by a NanoLED-440LH (100 ps, fwhm), while detection was collected on the same TBX detector above. The system can resolve lifetimes down to 40−50 ps. The fluorescence decay traces of the QD signal in the QD-dopamine conjugates (limited to a narrow window centered around the PL peak) with time were fitted to a three-exponential function:

$$I(t) = A_1 e^{-t/\tau_1} + A_2 e^{-t/\tau_2} + A_3 e^{-t/\tau_3} \quad (1)$$

where t is time and A_i is a weighting parameter associated with each decay time, τ_i. An average amplitude-weighted lifetime defined as:

$$\tau_{avg} = \frac{\sum A_i \tau_i^2}{\sum A_i \tau_i} \quad (2)$$

was extracted from the fit using Data Station software (Horiba Jovin-Yvon). The PL quenching efficiency, E, can be extracted from the steady-state or time-resolved fluorescence data, respectively, using the expressions:

$$E = 1 - \frac{F_{DA}}{F_D}, \text{ for steady-state fluorescence} \quad (3a)$$

and

$$E = 1 - \frac{\tau_{DA}}{\tau_D}, \text{ for time-resolved fluorescence} \quad (3b)$$

where F_{DA} and F_D designate the PL intensity measured for QD conjugates with and without dopamine redox complexes, respectively. Similarly, τ_{DA} and τ_D, respectively, designate the exciton lifetime measured for QD conjugates with and without dopamine.

Femtosecond Time-Resolved Transient Absorption Experimental Setup and Data Fitting. The laser system consists of a regeneratively amplified Ti:sapphire oscillator, which delivers 1 mJ pulse energies centered at 800 nm with a 1 kHz repetition rate. The measured pulse duration of the amplified pulse is typically 90 fs. The laser output is split by an optical wedge to generate the pump and probe beams. The pump beam is frequency doubled to produce approximately 200 μJ/pulse of 400 nm light. The excitation beam is focused to a 2 mm spot. The pump pulse energy used in these experiments was 500 nJ/pulse. The remaining laser amplifier output is focused onto a sapphire plate to generate visible and NIR continuum probe for differential transient absorption measurements. Time-resolved differential transient absorption spectra are collected with a commercial Helios transient absorption spectrometer (Ultrafast Systems LLC). Pump−probe dynamics are monitored by temporally delaying the probe beam with a linear translation stage capable of step sizes as small as 7 fs with a dynamic range extending to 3.2 ns. The instrument response function is determined from the nonresonant solvent response of the pump and probe laser pulses and is 150 fs in the visible and 350 fs in the NIR. Additional details of the femtosecond laser system used for this study and the TA as technique can be found in previous publications.[62]

Temporal integration of peaks measured in the transient absorption spectrum provided pump−probe kinetic traces. The best fits for the excited-state absorption features were three-exponential functions of the form:

$$S(t) = g(t) \sum c_n \times \exp\left(-\frac{t}{\tau_n}\right) \quad (4)$$

where $g(t)$ is a Gaussian function, which deconvolutes the instrument response to the overlap of the Gaussian pump and probe laser pulses, t is the time step with respect to the experimental zero, c_n is the amplitude coefficient of the nth component, and τ_n is the excitation lifetime of the nth component. τ_1 and τ_2 represent the internal relaxation processes, while τ_3 reflects the band edge relaxation. In the data analysis shown below, we will focus on changes measured for τ_3. The transient data were fit using an iterative least-squares approach written in house.[62,63]

RESULTS AND DISCUSSION

Conjugate Design. The present design was motivated by three goals: (1) The first was to provide hydrophilic QDs platforms with absorption and PL properties that exhibit little to no dependence on the environment pH. (2) Next is to assemble a construct where control over the conjugate architecture is achieved, which means control over the average number of redox active dopamines attached to a single QD and the distance between the nanocrystal center and redox complex location. The construct will also involve linkers between the QD and dopamine that are redox inactive. (3) The final goal was to use the above construct to probe the exact nature of the charge transfer interactions in these systems. Our aim is to develop an understanding of the quenching mechanism and its pH-dependence using steady-state and time-resolved fluores-

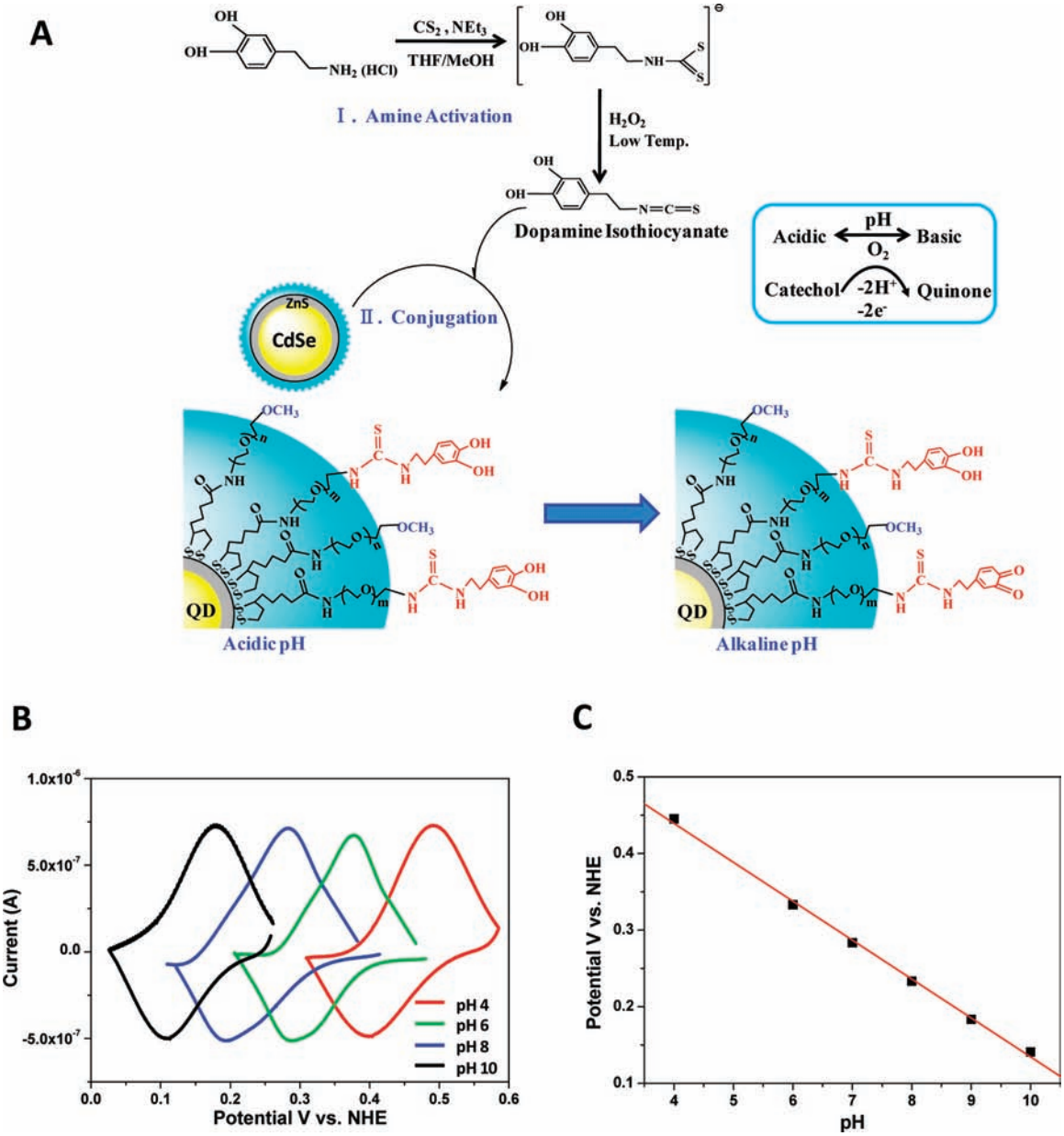

Figure 1. (A) Schematic representation of the dopamine-ITC synthesis and assembly of the QD-dopamine conjugates. A mixture of DHLA-PEG-OCH_3 and DHLA-PEG-NH_2 ligands is used to cap the QD surface. The average number of ethylene oxide monomers in the −PEG750−methoxy and −PEG600−NH_2 ligands used here are m = 12 and n = 15, respectively. Dopamine is first modified to amine reactive isothiocyanate (dopamine-ITC), before reaction with the amine-functionalized QDs. The inferred oxygen-catalyzed transformation of the catechol is shown in the inset and on the QD-conjugate. (B) Cyclic voltammograms collected from dispersions of dopamine-PEG-methoxy dispersed in varying pH buffers. (C) A plot of the potential for oxidation versus pH showing the expected linear behavior.

cence measurements. This will also allow us to eventually address some of the issues that have thus far remained unsolved. Indeed, pH stability (or inertness) of the hydrophilic QDs has often been overlooked in several studies. For example, it is known that core only nanocrystals such as CdTe or core−shell QDs with thin overcoating layer can exhibit pH-dependent PL properties,[64−66] and this may produce uncontrolled changes in the QD emission upon interactions with dopamine complexes. In our previous study, we relied on metal−histidine interactions and used a peptide linker appended with a hexa-histidine (His_6) tag to couple the QDs to dopamine.[52] Although versatile and simple, His-driven coordination onto metal ions tends to be pH-dependent, and it is weaker than thiol binding.[67] Also, rather weak quenching rates were measured with those QD-peptide-dopamine assemblies, even when large numbers of dopamine per QD-conjugate were used.[52]

In this study, we used a simpler model system to bring the dopamines in close proximity to the QD-surface. The DHLA-PEG-capped CdSe−ZnS QDs used exhibit no changes in the PL over the range pH 4−12, where most redox studies have been carried out. Figure 1A provides a schematic depiction of the QD-dopamine conjugates used along with the preparation steps involved. We used QDs cap-exchanged with a mixture of DHLA-PEG_{750}-OCH_3 and DHLA-PEG_{600}-NH_2 (QDs with mixed surface ligands) where the fraction of amine groups was varied.[19,60,61] The amine groups were reacted with dopamine-ITC to form a covalent isothiourea bond, which

dx.doi.org/10.1021/ja300724x | J. Am. Chem. Soc. 2012, 134, 6006−6017

has no pH-dependence. This provides an easy means to controllably tune the number of attached dopamine groups per nanocrystal. In addition, by using pH-insensitive QDs and relying on covalent coupling of the dopamine groups directly to the PEGylated cap, we guarantee that there are no other sources for pH-induced alterations in the optical properties of the QDs. We used a set of CdSe−ZnS nanocrystals having their first exciton peak at 552 nm and an emission centered at 572 nm (yellow color QDs). The PEG ligands DHLA-PEG$_{750}$-OCH$_3$ and DHLA-PEG$_{600}$-NH$_2$ were synthesized using our previously described protocols.[19,60] Additional details on the synthesis and characterization of the dopamine-ITC are provided in the Supporting Information.

Cyclic Voltammetry. The current versus applied voltage (CV) curves collected from solutions of dopamine-PEG-methoxy exhibit a well-defined oxidation peak that progressively shifts to lower values as the pH is increased (see Figure 1B). The oxidation peak exhibits the usual hysteresis measured when the applied potential is reversed. This pH-dependent shift in the oxidation peak is similar to previously reported data for dopamine.[52,68] They account for the usual oxygen driven two-electron two-proton transformation of the dopamine into quinone as the pH is increased.[47] The dopamine potential for oxidation versus pH exhibits a Nernstian response, which imparts a linear change with increasing pH:

$$E_f = E^0 - 0.059\left(\frac{h}{n}\right) \times \mathrm{pH} \quad (5)$$

where E_f is the average anodic and cathodic peak potentials, E^0 is the potential at pH 0, and h/n represents the proton to electron ratio. Our experimental data for dopamine-PEG-methoxy exhibited a linear behavior with pH with a slope $\cong$ 0.052 (close to the expected value at 25 °C shown in eq 5).[69] The negative shifts in the potential at alkaline pH's indicate a lower barrier to oxidation, and thus a shift of the equilibrium toward higher concentration of oxidized catechol, i.e., a propensity of dopamine to easily oxidize combined with an increase in the concentration of quinones in the medium.

Optimization of the Conjugate Valence. Like most chemical reactions, amine to isothiocyanate coupling, although reported to be effective, it is not 100% efficient;[70] often excess of one of the reagents is used to maximize the coupling yield. We thus probed the reaction conditions that provide the optimal coupling efficiencies of dopamine onto the amine-functionalized QDs. For this, we monitored the progression of the PL quenching efficiencies when different molar amounts of dopamine were reacted with the QDs for a given reaction time; reactions were carried out in DI water (pH $\approx$ 6.5). We used three sets of mixed surface QDs that present increasing fractions of DHLA-PEG-NH$_2$: 5%, 10%, and 15% DHLA-PEG-NH$_2$-QDs. Once the reaction is complete, the dispersions were subjected to one round of concentration/dilution using a membrane filtration device to remove unreacted dopamine prior to collection of the PL spectra. No aggregation buildup was observed in any of the samples even after several weeks of storage.

Figure 2A shows the typical progression in the QD PL with increasing molar concentration of dopamine for the set of 5% DHLA-PEG-NH$_2$-QDs (the QD concentration is fixed); the fluorescence image of selected dispersions of these conjugates under UV illumination is shown in the inset of Figure 2A. High levels of PL quenching were measured in the presence of increasing concentration of dopamine (Figure 2B). Similar

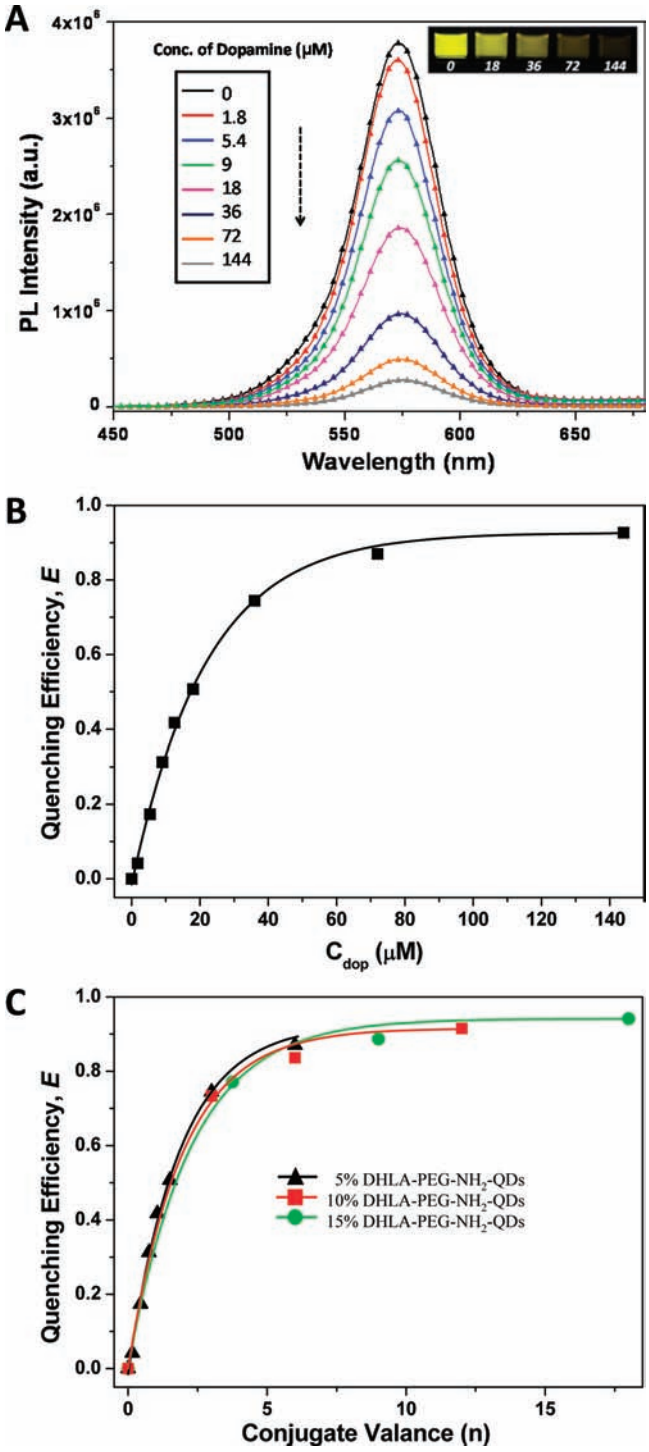

Figure 2. (A) Progression of the PL spectra collected from QD-dopamine conjugates dispersed in DI water for increasing molar concentration of added dopamine-ITC, n. The dopamine concentration is given prior to removal of excess unreached dopamine-ITC using a membrane filtration device. Inset: A fluorescence image of selected dispersions of these QD-conjugates under UV illumination. (B) Quenching efficiency versus C_{dop} for the sets of 5% DHLA-PEG-NH$_2$-QDs. (C) Cumulative plots of the quenching efficiency versus valence n for the three sets of DHLA-PEG-NH$_2$-QDs used: 5%, 10%, and 15% DHLA-PEG-NH$_2$-QDs. Fits of the data to eqs 6 and 7 are shown.

trends were also observed for the 10% and 15% of DHLA-PEG-NH$_2$-QDs, although higher efficiencies were overall measured

dx.doi.org/10.1021/ja300724x | J. Am. Chem. Soc. 2012, 134, 6006−6017

for those dispersions. For example, we measured a PL quenching efficiency that exceeds 85% for all samples at dopamine-to-QD molar ratios of 90; that efficiency exceeds 90% (nearing saturation) at higher ratios (Figure 2 and Supporting Information). The ratio values given above correspond to the molar concentration of dopamine added, before removal of unreacted dopamine-ITC from the medium.

We should stress that conversion from relative molar concentrations of dopamine and QDs to ratios between dopamine-ITC and amine (or number of dopamines per QD) is not straightforward, because it requires a measure of the number of ligands per nanocrystal. In fact, accurate estimate of the number of ligands, or functional groups, per nanoparticle for a variety of inorganic nanocrystals (e.g., QDs and metal nanoparticles) has been a challenge.[18,71−76] For our present sample configuration, we refer to a recent study where we estimated the number of TA-PEG (polyethylene glycol-appended thioctic acid) ligands per AuNP. We prepared a set of mixed ligand AuNPs presenting increasing fractions of TA-PEG-Maleimide per nanoparticle and combined the use of cysteine-terminated peptide-dye, maleimide-to-cysteine coupling, and optical absorption to extract an estimate for the foot print area (FPA) per ligand.[72] We found that TA-PEG ligands have an average FPA of 1.25 nm^2 per ligand, regardless of the NP size. Assuming that the density of ligands is the same for ZnS-overcoated CdSe QDs and AuNPs, using the above FPA and accounting for difference in nanocrystal size, we estimate that the total number of ligands per QD is ∼120. This would result in a number of amines per QD equal to 6, 12, and 18 for 5%, 10%, and 15% DHLA-PEG-NH_2-QDs, respectively. We will be referring interchangeably to molar excess of dopamine (for a fixed QD concentration) or dopamine valence per QD-conjugate.

The steady-state data are further supported by the time-resolved fluorescence measurements, where shortening of the QD exciton lifetime with increasing dopamine concentration was measured (see Supporting Information, Figure S2). The PL decay profiles were monitored at the emission peak (572 nm) and fitted to a three-exponential function shown in eq 3b. The efficiencies obtained from the time-resolved data were overall comparable to those derived from the steady-state fluorescence as shown in Figure 2B.

In contrast, control experiments performed using 0% DHLA-PEG-NH_2-QDs (i.e., DHLA-PEG-methoxy-capped QDs) mixed with free dopamine showed substantially smaller PL losses. For instance, a linear behavior of the PL loss was measured as a function of the dopamine molar concentration, with ∼35% PL quenching measured at the highest concentration (corresponding to dopamine-to-QD ratio: 180:1). Following one round of filtration, the residual PL loss was smaller than 5%. This behavior is characteristic of solution phase quenching driven by collision interactions; more details are provided in the Supporting Information (Figure S3).

These results combined indicate that indeed covalent coupling of dopamine onto the QDs has been realized using our present strategy and that the number of redox active groups on a QD can be further tuned by changing the fraction of amine groups on a nanocrystal and/or varying the molar concentration of dopamine added to the reaction mixture; we expect a linear relationship between the initial dopamine-ITC concentration, C_{dop}, added and the number of redox groups attached to the QD, n, following the removal of excess unreacted dopamine. The proportionality relationship between n and C_{dop} is a direct result of the first-order bimolecular reaction analysis.[67] The present conjugate design is expected to provide a constant average separation distance between the QD and proximal dopamines. For such configuration, the dependence of the quenching efficiency (defined in eq 3) on the number of attached dopamines per QD follows the expression:

$$E = \frac{\alpha n}{\alpha n + K} \tag{6}$$

where α is an experimental constant (here it depends on the matching between the redox levels of QD and dopamine) and K accounts for the effects of separation distance. This expression is similar to the one developed for Förster resonance energy transfer between a central QD and n dyes arrayed at a fixed distance from the QD center.[35,36,77] Because n is proportional to the concentration of dopamine-ITC used (see above), a similar expression can be written for E versus C_{dop}:

$$E = \frac{\alpha' C_{dop}}{\alpha' C_{dop} + K} \tag{7}$$

α' is related to α above. A cumulative plot of the PL quenching efficiency versus C_{dop} for three sets of QD dispersions is shown in Figure 2C. The steady-state quenching data can indeed be easily fit to eq 7. Moreover, we found that such fit yields similar values of K/α' for the three sets of amine-QDs used, with K/α' = 14.3, 13.5, and 15.2 for 5%, 10%, and 15% DHLA-PEG-NH_2-QDs, respectively. The consistent values for K/α' extracted for the three sets of QDs clearly indicate that the number of coupled dopamine per QD tracks the concentration of dopamine-ITC used as expected. In addition, because saturation in the quenching efficiency is observed at higher C_{dop}/C_{QD} ratios, we will assume hereafter that at C_{dop}:$C_{QD} \geq$ 90:1 (added dopamine prior to filtration), essentially all amines on the QD have been activated, yielding n = 6, 12, and 18 for 5%, 10%, and 15% DHLA-PEG-NH_2-QDs, respectively.

Effects of Solution pH. We now focus on the effects of varying the buffer pH on the PL properties of the conjugates and probe changes in the steady-state and time-resolved fluorescence. All of the conjugates used were prepared using an initial dopamine-to-QD ratio of 45:1 (prior to removal of the excess unreacted dopamine-ITC). This ratio was chosen because it allows us to evaluate changes in the dispersion properties far enough from the saturation regime (where the PL losses exceed 85%); probing the system away from saturation quenching allow measurements over a regime where larger relative changes in PL emission can be achieved. Figure 3A shows a typical progression of the PL spectra over the pH range 4−10 (using 10 mM phosphate buffers) for the set of 5% DHLA-PEG-NH_2-QDs. Clearly, the steady-state PL undergoes a pronounced but progressive loss as the pH is increased. This PL loss is complemented with the progressive shortening in the luminescence lifetime with increasing solution pH (Figure 3B). Furthermore, we found that in the reverse configuration where the conjugates are initially prepared in alkaline buffer, then the pH is reduced to acidic, the PL undergoes a progressive recovery that is also pH-dependent (see Figure 3C).

Cumulative plots for the relative change in PL with the solution pH, along with an image of the conjugate dispersions at pH 6.5, are shown in Figure 4. The data indicate that a similar trend is found for all three sets of QD-conjugates used, although consistently larger PL losses were measured for solutions made with 10% and 15% DHLA-PEG-NH_2-QDs,

dx.doi.org/10.1021/ja300724x | J. Am. Chem. Soc. 2012, 134, 6006−6017

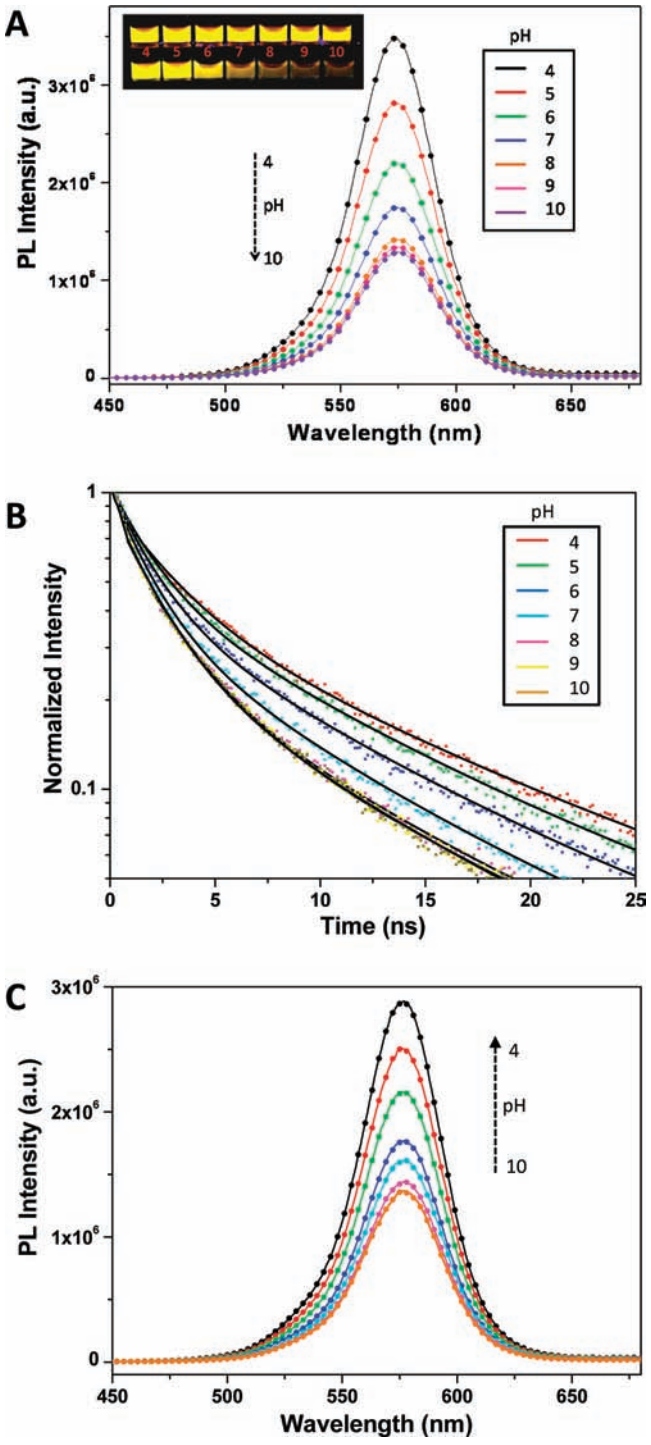

Figure 3. (A) Steady-state fluorescence spectra collected from solutions of QD-dopamine conjugates (using a nominal dopamine-to-QD molar ratio of 45:1 prior to purification) for increasing pH values ranging from 4 to 10. Inset: Images of QDs in the absence of dopamine (top) and of QD-dopamine conjugates (bottom) dispersed in different pH buffers. (B) Time-resolved PL decays for dispersion of QD-dopamine conjugates (45:1 dopamine to QD) in different buffers ranging from pH 4 to 10. (C) Progression of the PL spectra versus decreasing pH (reverse configuration of data shown in (A)). The conjugates were initially dispersed in pH 10 buffer, and then 40 μL aliquots of this stock solution were mixed with the desired pH buffer (960 μL) before the spectra were collected.

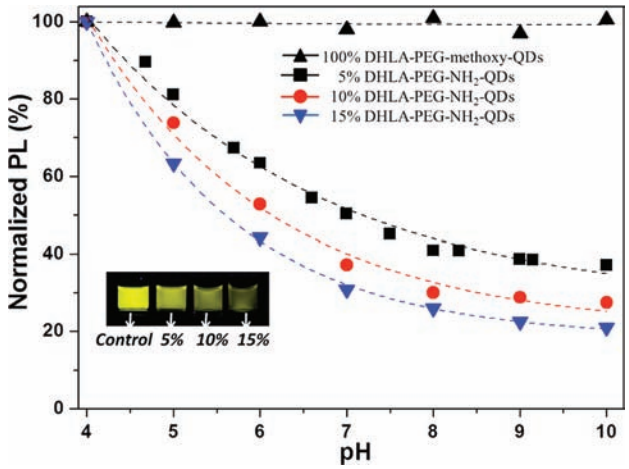

Figure 4. Integrated PL intensity for the pH range 4−10 normalized (as percentage) with respect to the initial values at pH 4; the conjugate valence increases with the fraction of amine-appended ligand used. Inset: Image of these dispersions in DI water (pH 6.5).

where higher conjugate valences are anticipated. These observations are supported by time-resolved fluorescence data, where more pronounced changes in the exciton lifetime were measured as a function of pH for the QD-conjugates with higher dopamine valence. The PL spectra along with the time-resolved data for those dispersions are provided in the Supporting Information (Figures S4 and S5). In contrast, there are no measurable changes in the PL signal for control dispersions containing DHLA-PEG-OCH_3-QDs (see Figure 4).

We should add that fluorescence spectra collected from dispersions of QD-dopamine conjugates to which excess hydrazine (at 1% by volume) was added showed no difference in the quenching properties as compared to hydrazine-free dispersions (see the Supporting Information). Hydrazine was believed to ensure prereduction of dopamine in the conjugates.[52] This indicates that at pH 4, equilibrium favors the presence of the reduced form of dopamine.

Investigating the Importance of Oxygen. It is widely accepted that the pH-induced oxidation of dopamine (transformation of the hydroxyl groups) heavily relies on the presence of oxygen solubilized in the medium; that is, oxidation of dopamine is an oxygen-catalyzed transformation.[47,78] To test this rationale and to gain a deeper understanding of the role that oxygen plays in controlling the pH-dependent charge transfer, we carried out two sets of experiments. (1) In the first, we compared side-by-side the PL quenching of QD-dopamine conjugates dispersed in "regular" DI water and buffer solutions at varying pH's (referred to hereafter as oxygen-rich solutions), and in DI water and buffers through which argon has been bubbled for ∼3−3.5 h (referred to as oxygen-depleted/free dispersions); in the latter experiments, conjugation and manipulation of the dispersions have been carried out in these oxygen-free buffers and using a dopamine-ITC-to-QD ratio (nominal) of 45:1. (2) In the second, we measured changes in the absorption properties of dopamine-PEG-OCH_3 dispersed in regular (oxygen-rich) buffers at several pH's and compared them to the spectra collected from dispersions in argon-saturated buffers. Figure 5A shows a plot of the normalized fluorescence intensity versus pH over the range pH 4−10 in both conditions; the initial value of the PL signal at pH 4 is taken as 100%. We should, however, note that there is a small (∼10%) PL loss measured at pH 4 for the oxygen-rich

dx.doi.org/10.1021/ja300724x | J. Am. Chem. Soc. 2012, 134, 6006−6017

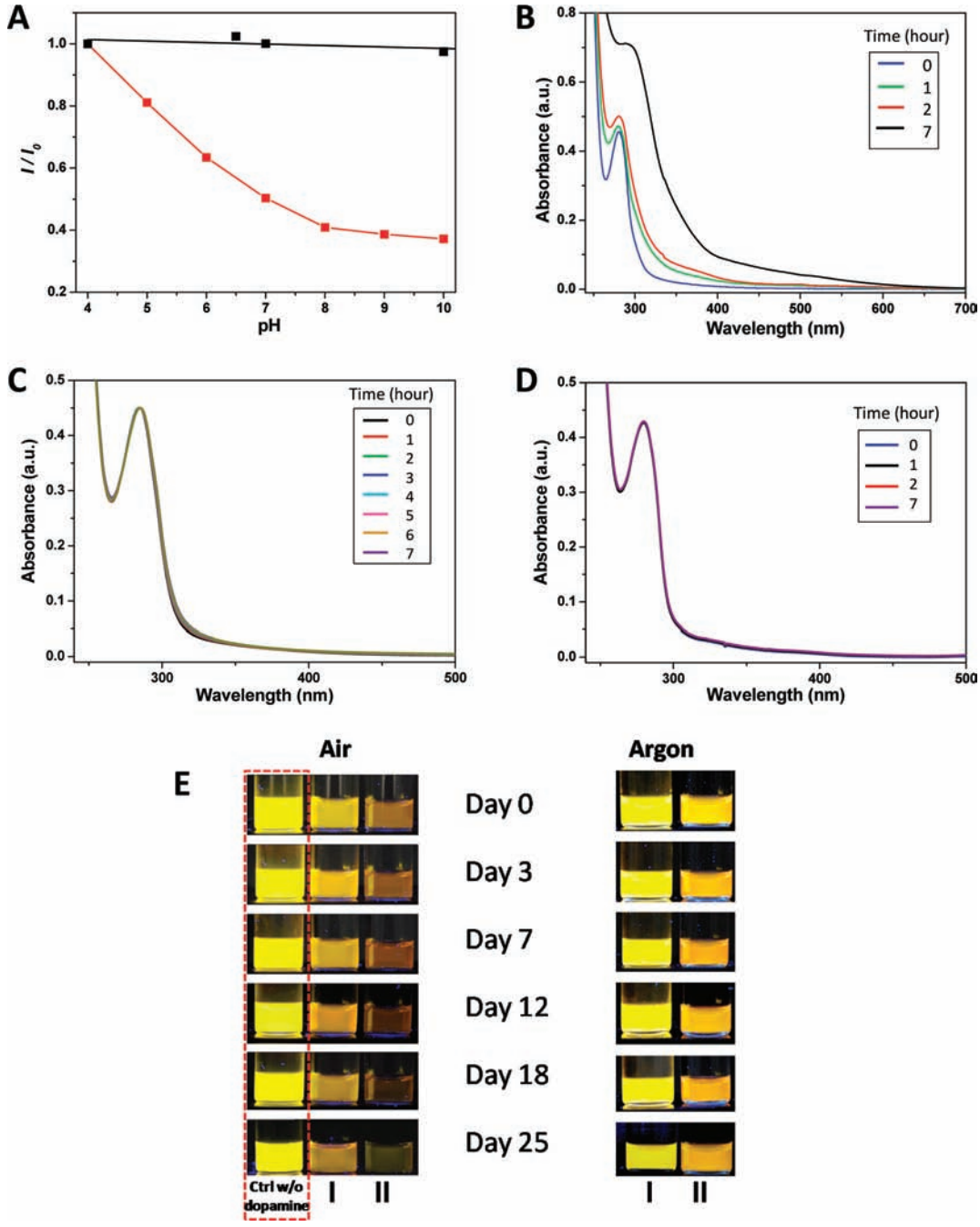

Figure 5. (A) Progression of the fluorescence intensity versus pH for QD-dopamine conjugates (nominal C_{dop}/C_{QD} = 45) dispersed in oxygen-rich buffers (red ■) and in oxygen-depleted buffers (black ■). (B–D) Representative absorbance spectra collected from solutions of dopamine-PEG-methoxy with elapsed time in oxygen-rich buffers at pH 10 (B), and in oxygen-depleted buffers at pH 10 (C) and at pH 4 (D). (E) Images of QD and QD-conjugate dispersions in oxygen-rich buffer (left) and in oxygen-depleted buffers (right) with two different dopamine-ITC concentrations over several days of storage; QDs = 0.8 μM and C_{dop} = 18 (I) and 144 μM (II) (values are provided prior to removal of excess unreacted materials via filtration).

and oxygen-free dispersions as compared to the unconjugated QD dispersions. This reflects a residual quenching due to the presence of dopamine around the QD even in acidic buffers, where the equilibrium is expected to favor the reduced form of dopamine (see more details below). Clearly, a pronounced and pH-dependent quenching (as high as 60%) is measured for the conjugates in oxygen-rich alkaline buffers (as compared to the initial value at pH 4). In contrast, for QD-dopamine conjugates dispersed in oxygen-depleted buffers, negligible change in the PL intensity is measured for acidic and alkaline pH as compared to the value at pH 4. These differences were complemented with TR fluorescence experiments where little to no change in the exciton lifetime was measured for the oxygen-depleted solutions (see the Supporting Information). To complement these results, we monitored changes in the absorption spectra of dopamine-PEG-methoxy at pH 4, 7, 9, and 10. We found that a substantial change in the absorption peak at 280 nm takes place at higher pH's, and the rate of change is accelerated in alkaline buffers before reaching saturation (after up to 7 h). Such transformation in the absorption features is attributed to

dx.doi.org/10.1021/ja300724x | J. Am. Chem. Soc. 2012, 134, 6006–6017

progressive oxidation of the dopamine to quinone; that is, the concentration of quinone in the dispersion is increased at alkaline pH. However, there is no change in the absorption spectrum of dopamine with pH or time for dopamine-PEG-methoxy dissolved in argon-purged buffers, indicating that the rate of oxidation has been drastically reduced when solubilized oxygen is removed (see Figure 5C,D and Supporting Information). These findings combined with the cyclic voltammetry data prove that oxygen plays a crucial role in the pH-dependent oxidation of dopamine and the ensuing quenching of the QD emission.

Mechanism for the Charge Transfer-Induced Quenching of QD Photoemission. There are four main features that emerge from the above set of data: (1) Arraying several dopamine groups around the QD surface induces a loss in its photoemission, with a quenching efficiency that tracks the valence of the QD-dopamine conjugate. However, the rate of quenching as verified by both steady-state and time-resolved fluorescence measurements strongly depends on the pH of the buffer used, with substantially more pronounced PL losses measured in alkaline solutions than in acidic ones. (2) In oxygen-free buffers, the additional PL losses measured at alkaline pH (as compared to those measured at pH 4) are negligible, which implies that the pH-dependent interaction mechanism driving the PL change is oxygen-catalyzed. (3) There is a small residual quenching at pH 4 for both sets of dispersions (oxygen-rich and oxygen-free buffers). (4) These results cannot be attributed to Förster resonance energy transfer between the QDs and dopamine, because there is no measurable spectral overlap between the QD emission and dopamine absorption; the latter absorption is weak and limited to the UV region of the spectrum (see Figure 5).

The CV data shown in Figure 1B indicate that equilibrium favors easier oxidation of dopamine at higher pH, as reflected by the decrease in the oxidation potential with increasing pH. This implies that in alkaline buffers equilibrium favors electron transfer from the fully or partially reduced dopamine to the QD. Conversely, a more favorable oxygen-catalyzed transformation in alkaline buffers implies that the concentration of quinone increases at basic pH's, which naturally favors electron transfer from photoexcited QDs to the redox complex; quinone is by nature a better electron acceptor.[79,80] These observations may somewhat be contradictory, but they reflect the fact that what we measure results from interactions of a QD with two distinct complexes (at least) that coexist in the same conjugate. Electron transfer to an unexcited QD should produce a partial bleaching of the first exciton absorption in addition to PL quenching.[35,81,82] Indeed, we measured a bleaching, although very small, of the first QD absorption peak at alkaline pH's, which supports the above rationale that the reduced dopamine is a more favorable electron donor (see the Supporting Information).

To complement our findings and to gain a better insight into the mechanism that drives the pH-dependent PL quenching, we carried out transient absorption (TA) measurements on two representative sets of dispersions: QD-dopamine conjugates and unconjugated QDs dispersed in pH 4 and pH 10 buffers; the QD dispersions provided control samples. We used QD-conjugate with a nominal valence of 6 dopamine complexes per nanocrystal (set of 5% DHLA-PEG-NH_2-QDs). Time progression of the differential absorption (ΔAbs) spectra for these samples is shown in Figure 6. Here, we focus on the contribution in the NIR spectral region 900−1400 nm, which

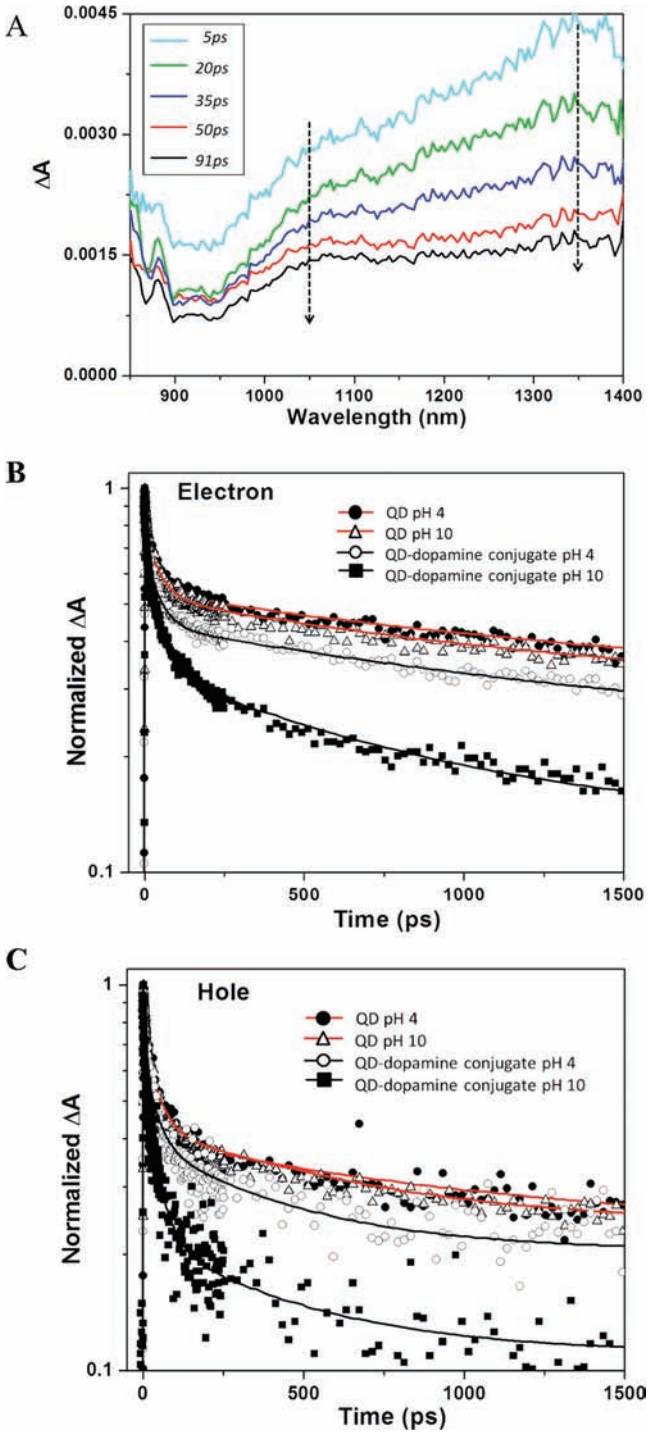

Figure 6. (A) Wavelength-resolved TA spectra plotted at several pump−probe delay times for QD-dopamine conjugate at pH 10. (B) Time-resolved decay of the TA signal recorded at 1050 nm probe wavelength corresponding to the electron. (C) Decay recorded at 1350 nm corresponding to the hole. Substantial changes in the relaxation are measured for the electron and hole in alkaline buffers (pH 10) as compared to QDs control. Conversely, only marginal changes are measured for the conjugates at pH 4 as compared to QDs only. The solid lines are fit to the data using eq 4.

allows one to probe changes in the intraband transitions of the electron and hole of a photoexcited QD in the conjugates. These are extracted from the positive contributions to the differential absorption at 1050 and 1350 nm, respectively. We

dx.doi.org/10.1021/ja300724x | J. Am. Chem. Soc. 2012, 134, 6006−6017

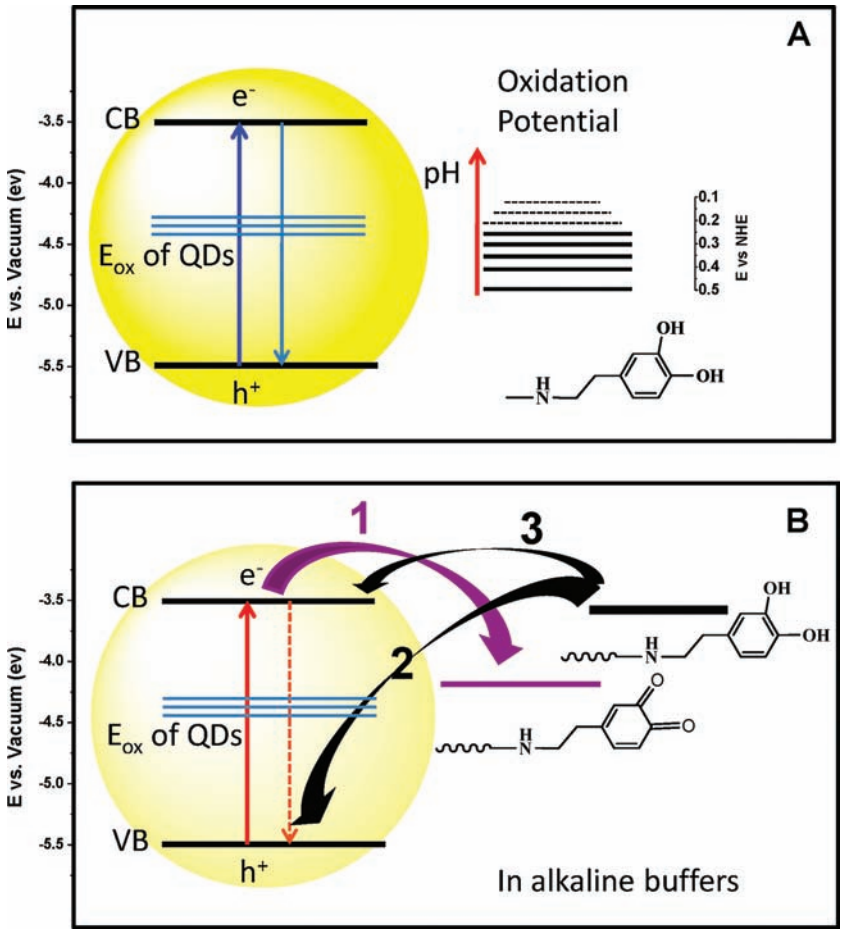

Figure 7. (A) Progression of the dopamine potential for oxidation with increasing pH derived from the CV data shown in Figure 1. The oxidation potential of the QDs (E_{ox} of QDs) along with the corresponding energy levels (e.g., E_{ox} of QDs, CB, and VB) were reproduced from refs 32,35,83,84. (B) Schematic representation of the proposed relaxation mechanisms for the electron and hole pair in the system in alkaline buffers: **1** designates electron transfer from a photoexcited QD to quinone; **2** designates electron transfer from dopamine to the valence band of a photoexcited QD; while **3** accounts for the electron transfer from dopamine to an unexcited QD. Increasing concentration of quinones favors higher electron transfer from the QD to proximal oxidized complex, while oxidation of the reduced dopamine promotes easier transfer of electron to the valence band of the QD.

found that the time-decays of both TA signals experience substantial change as the solution pH is switched from 4 to 10; the changes for unconjugated QDs are negligible. Similarly, only minor changes are measured for the conjugates at pH 4 as compared to the control samples. The time-resolved TA data, although preliminary, are very informative and indicate that both electron and hole contributions exhibit faster relaxation(s) in the presence of dopamine in alkaline solutions (pH 10) (see Figure 6B,C). For example, at pH 10, τ_3 measured for the QD-dopamine conjugates changes from 800 to 450 ps for the hole and from 1230 to 760 ps for the electron, as compared to QDs control. Similarly, when the pH is increased from 4 to 10, τ_3 measured for the QD-conjugates changes from 1530 to 760 ps for the electron and from 650 to 450 ps for the hole, respectively. The rapid increase in the relaxation rates of both carriers (electron and hole) upon conjugation to dopamine in alkaline buffers proves that charge transfer in these complexes affects the electron and hole alike.

On the basis of these data, we attribute the present observations to a combination of three processes that occur simultaneously: (1) transfer of electrons from a photoexcited QDs to the lowest unoccupied molecular orbital of the proximal quinone acceptor; (2) electron transfer from the reduced (or partially reduced) dopamines in the construct to the valence band of the phoexcited QDs; and (3) weak transfer of electron from dopamine to an unexcited QD. A schematic diagram showing the proposed charge transfer mechanism for these conjugates as the pH of the buffer is changed from acidic to basic is shown in Figure 7. Pathways 1 and 2 combined result in annihilation of the QD exciton. This mechanism is consistent with the above set of data, including CV curves and the fluorescence data. The major effect of changing the buffer pH from acidic to alkaline is to shift the equilibrium by lowering the oxidation potential of the complexes, and consequently increasing the overall concentration of quinones in the solution. Thus, as the pH is increased, both transfer rates are enhanced. Lower potential for oxidation enhances the rate of charge transfer from dopamine to the valence band of the photoexcited QD. Similarly, the concentration of proximal quinone in the medium is increased at basic pH, which favors electron transfer from photoexcited QDs to proximal quinones. These relaxation channels combined enhance the rate of PL quenching of the QD when the dispersion pH is increased from acidic to basic. This produces high levels of quenching efficiencies as observed for our present set of QD-dopamine conjugates.

We should compare the present set of data to those previously reported by our group using QD-dopamine conjugates assembled via peptide linkers. The rate of quenching

dx.doi.org/10.1021/ja300724x | J. Am. Chem. Soc. 2012, 134, 6006−6017

measured for the present constructs is substantially higher than what we reported in ref 52, even though much smaller conjugate valences were used. Furthermore the dependence of the PL loss on the number of dopamine-peptides used was essentially linear, indicating that either large separation distances were involved, or a not so effective conjugation; this may be enhanced by the fact that metal-to-histidine coordination is pH-sensitive and tends to become weaker at lower pH. The present design avoided that issue by relying on covalent coupling, while guaranteeing shorter separation distances and uses PEG linkers as inert bridges instead of peptides. We also saw only marginal effects of adding hydrazine to the solution on the quenching properties of the QD-conjugates. Thus, our present conjugates provided a better model system to probe the interactions between QDs and the redox active dopamine. Combined with the TA measurements, it allowed us to develop a more coherent understanding of the charge transfer interactions in these systems.

CONCLUSIONS

We investigated the charge transfer interactions between luminescent QDs and redox active dopamine. For this we used DHLA-PEG-capped QDs that presented a small but controllable number of terminal reactive amines, and coupled them to dopamine-ITC. This sample configuration has a few unique advantages: (1) it provided a construct where a single donor can simultaneously interact with several covalently bound acceptors, all via an inert PEG linker; (2) the interactions could be controlled by varying the number of dopamines per QD-conjugate or/and the buffer pH; and (3) it allowed us to probe the effects of the conjugate valence as well as pH, all on a biologically inert QD platform. Combining steady-state and time-resolved fluorescence, we measured pronounced PL quenching for the QD-dopamine assemblies. We found that the PL loss was affected by the conjugate valence, and quenching substantially increased in alkaline pH's. We also found that oxygen depletion from the solution reduced the PL quenching to essentially nil. Transient absorption measurements showed that the relaxation of the intraband transitions of the electron and hole alike was substantially altered when the pH was switched from 4 to 10. We attribute these observations to charge transfer interactions between the central QD and proximal dopamines in the conjugates. Increasing the pH from 4 to 10 decreases the dopamine oxidation potential, while shifting the equilibrium between the oxidized and reduced forms of the complex progressively favors higher concentration of quinone in the medium. These two forms of the complex have very different electronic behaviors; the reduced catechol becomes a better electron donor with increasing pH, while quinone naturally provides a better electron acceptor. This produces a conjugate where a photoexcited QD can simultaneously transfer an electron from the CB to a quinone, while a reduced catechol transfers an electron via two pathways: (1) directly into the conduction band of a QD producing a partial bleaching of the first exciton peak, and/or (2) transfer of an electron to the VB of a photoexcited QD, annihilating the existing hole. These two relaxation channels are nonradiative and cumulative; when combined they enhance the rate of QD PL quenching in basic pH, producing rather high levels of losses even at low conjugate valences. Further investigation will focus on additional parameters, such as the effects of separation distance and applying these conjugates as in vivo pH sensor.

ASSOCIATED CONTENT

Supporting Information

Additional experimental details. This material is available free of charge via the Internet at http://pubs.acs.org.

AUTHOR INFORMATION

Corresponding Author

mattoussi@chem.fsu.edu

Present Address

[†]Department of Chemistry "G. Ciamician", University of Bologna, 40126 Bologna, Italy.

Notes

The authors declare no competing financial interest.

ACKNOWLEDGMENTS

We thank FSU, the National Science Foundation (Grant No. 1058957), and Pfizer for financial support. H.B.N. was supported by a fellowship from the National Research Foundation of Korea (D00074). K.L.K. gratefully acknowledges the U.S. Air Force Office of Scientific Research for financial support under AFOSR award no. FA9550-1-1-0300. We thank Guocan Li and Professor Michael Shatruk for assistance with the cyclic voltammetry measurements.

REFERENCES

(1) Murray, C. B.; Norris, D. J.; Bawendi, M. G. *J. Am. Chem. Soc.* **1993**, *115*, 8706.

(2) Murray, C. B.; Kagan, C. R.; Bawendi, M. G. *Annu. Rev. Mater. Sci.* **2000**, *30*, 545.

(3) Peng, X.; Manna, L.; Yang, W.; Wickham, J.; Scher, E.; Kadavanich, A.; Alivisatos, A. P. *Nature* **2000**, *404*, 59.

(4) Klimov, V. I. *Nanocrystal Quantum Dots*, 2nd ed.; CRC Press: Boca Raton, FL, 2010.

(5) Talapin, D. V.; Lee, J. S.; Kovalenko, M. V.; Shevchenko, E. V. *Chem. Rev.* **2010**, *110*, 389.

(6) Rogach, A. L.; Talapin, D. V.; Shevchenko, E. V.; Kornowski, A.; Haase, M.; Weller, H. *Adv. Funct. Mater.* **2002**, *12*, 653.

(7) Alivisatos, A. P. *J. Phys. Chem.* **1996**, *100*, 13226.

(8) Reiss, P.; Protière, M.; Li, L. *Small* **2009**, *5*, 154.

(9) Hines, M. A.; Guyot-Sionnest, P. *J. Phys. Chem.* **1996**, *100*, 468.

(10) Dabbousi, B. O.; RodriguezViejo, J.; Mikulec, F. V.; Heine, J. R.; Mattoussi, H.; Ober, R.; Jensen, K. F.; Bawendi, M. G. *J. Phys. Chem. B* **1997**, *101*, 9463.

(11) Reiss, P.; Bleuse, J.; Pron, A. *Nano Lett.* **2002**, *2*, 781.

(12) Deka, S.; Quarta, A.; Lupo, M. G.; Falqui, A.; Boninelli, S.; Giannini, C.; Morello, G.; De Giorgi, M.; Lanzani, G.; Spinella, C.; Cingolani, R.; Pellegrino, T.; Manna, L. *J. Am. Chem. Soc.* **2009**, *131*, 2948.

(13) Susumu, K.; Uyeda, H. T.; Medintz, I. L.; Pons, T.; Delehanty, J. B.; Mattoussi, H. *J. Am. Chem. Soc.* **2007**, *129*, 13987.

(14) Muro, E.; Pons, T.; Lequeux, N.; Fragola, A.; Sanson, N.; Lenkei, Z.; Dubertret, B. *J. Am. Chem. Soc.* **2010**, *132*, 4556.

(15) Yildiz, I.; Deniz, E.; McCaughan, B.; Cruickshank, S. F.; Callan, J. F.; Raymo, F. M. *Langmuir* **2010**, *26*, 11503.

(16) Smith, A. M.; Nie, S. *J. Am. Chem. Soc.* **2008**, *130*, 11278.

(17) Gerion, D.; Pinaud, F.; Williams, S. C.; Parak, W. J.; Zanchet, D.; Weiss, S.; Alivisatos, A. P. *J. Phys. Chem. B* **2001**, *105*, 8861.

(18) Liu, W.; Howarth, M.; Greytak, A. B.; Zheng, Y.; Nocera, D. G.; Ting, A. Y.; Bawendi, M. G. *J. Am. Chem. Soc.* **2008**, *130*, 1274.

(19) Susumu, K.; Mei, B. C.; Mattoussi, H. *Nat. Protoc.* **2009**, *4*, 424.

(20) Pellegrino, T.; Manna, L.; Kudera, S.; Liedl, T.; Koktysh, D.; Rogach, A. L.; Keller, S.; Rädler, J.; Natile, G.; Parak, W. J. *Nano Lett.* **2004**, *4*, 703.

(21) Yu, W. W.; Chang, E.; Falkner, J. C.; Zhang, J.; Al-Somali, A. M.; Sayes, C. M.; Johns, J.; Drezek, R.; Colvin, V. L. *J. Am. Chem. Soc.* **2007**, *129*, 2871.
(22) Wu, H.; Zhu, H.; Zhuang, J.; Yang, S.; Liu, C.; Cao, Y. C. *Angew. Chem., Int. Ed.* **2008**, *47*, 3730.
(23) Yeh, Y.-C.; Patra, D.; Yan, B.; Saha, K.; Miranda, O. R.; Kim, C. K.; Rotello, V. M. *Chem. Commun.* **2011**, *47*, 3069.
(24) Alivisatos, P. *Nat. Biotechnol.* **2004**, *22*, 47.
(25) Michalet, X.; Pinaud, F. F.; Bentolila, L. A.; Tsay, J. M.; Doose, S.; Li, J. J.; Sundaresan, G.; Wu, A. M.; Gambhir, S. S.; Weiss, S. *Science* **2005**, *307*, 538.
(26) Medintz, I. L.; Uyeda, H. T.; Goldman, E. R.; Mattoussi, H. *Nat. Mater.* **2005**, *4*, 435.
(27) Zrazhevskiy, P.; Sena, M.; Gao, X. H. *Chem. Soc. Rev.* **2010**, *39*, 4326.
(28) Somers, R. C.; Bawendi, M. G.; Nocera, D. G. *Chem. Soc. Rev.* **2007**, *36*, 579.
(29) Zhang, Y.; Schnoes, A. M.; Clapp, A. R. *ACS Appl. Mater. Interfaces* **2010**, *2*, 3384.
(30) Stewart, M. H.; Susumu, K.; Mei, B. C.; Medintz, I. L.; Delehanty, J. B.; Blanco-Canosa, J. B.; Dawson, P. E.; Mattoussi, H. *J. Am. Chem. Soc.* **2010**, *132*, 9804.
(31) Dubois, F.; Mahler, B.; Dubertret, B.; Doris, E.; Mioskowski, C. *J. Am. Chem. Soc.* **2007**, *129*, 482.
(32) Amelia, M.; Impellizzeri, S.; Monaco, S.; Yildiz, I.; Silvi, S.; Raymo, F. M.; Credi, A. *ChemPhysChem* **2011**, *12*, 2280.
(33) Dubach, J. M.; Harjes, D. I.; Clark, H. A. *J. Am. Chem. Soc.* **2007**, *129*, 8418.
(34) Wolcott, A.; Gerion, D.; Visconte, M.; Sun, J.; Schwartzberg, A.; Chen, S. W.; Zhang, J. Z. *J. Phys. Chem. B* **2006**, *110*, 5779.
(35) Medintz, I. L.; Pons, T.; Trammell, S. A.; Grimes, A. F.; English, D. S.; Blanco-Canosa, J. B.; Dawson, P. E.; Mattoussi, H. *J. Am. Chem. Soc.* **2008**, *130*, 16745.
(36) Snee, P. T.; Somers, R. C.; Nair, G.; Zimmer, J. P.; Bawendi, M. G.; Nocera, D. G. *J. Am. Chem. Soc.* **2006**, *128*, 13320.
(37) Sykora, M.; Petruska, M. A.; Alstrum-Acevedo, J.; Bezel, I.; Meyer, T. J.; Klimov, V. I. *J. Am. Chem. Soc.* **2006**, *128*, 9984.
(38) Chen, Y.; Thakar, R.; Snee, P. T. *J. Am. Chem. Soc.* **2008**, *130*, 3744.
(39) Knowles, K. E.; Tice, D. B.; McArthur, E. A.; Solomon, G. C.; Weiss, E. A. *J. Am. Chem. Soc.* **2010**, *132*, 1041.
(40) Amelia, M.; Font, M.; Credi, A. *Dalton Trans.* **2011**, *40*, 12083.
(41) Impellizzeri, S.; Monaco, S.; Yildiz, I.; Amelia, M.; Credi, A.; Raymo, F. M. *J. Phys. Chem. C* **2010**, *114*, 7007.
(42) Medintz, I. L.; Mattoussi, H. *Phys. Chem. Chem. Phys.* **2009**, *11*, 17.
(43) Yildiz, I.; Deniz, E.; Raymo, F. M. *Chem. Soc. Rev.* **2009**, *38*, 1859.
(44) Giros, B.; Caron, M. G. *Trends Pharmacol. Sci.* **1993**, *14*, 43.
(45) Usiello, A.; Baik, J. H.; Rouge-Pont, F.; Picetti, R.; Dierich, A.; LeMeur, M.; Piazza, P. V.; Borrelli, E. *Nature* **2000**, *408*, 199.
(46) Darvas, M.; Palmiter, R. D. *J. Neurosci.* **2010**, *30*, 1158.
(47) Klegeris, A.; Korkina, L. G.; Greenfield, S. A. *Free Radical Biol. Med.* **1995**, *18*, 215.
(48) Tomlinson, I. D.; Mason, J. N.; Blakely, R. D.; Rosenthal, S. J. *Bioorg. Med. Chem. Lett.* **2006**, *16*, 4664.
(49) Clarke, S. J.; Hollmann, C. A.; Zhang, Z. J.; Suffern, D.; Bradforth, S. E.; Dimitrijevic, N. M.; Minarik, W. G.; Nadeau, J. L. *Nat. Mater.* **2006**, *5*, 409.
(50) Gill, R.; Freeman, R.; Xu, J. P.; Willner, I.; Winograd, S.; Shweky, I.; Banin, U. *J. Am. Chem. Soc.* **2006**, *128*, 15376.
(51) Kar, S.; Banerjee, S.; Perez, J. M.; Santra, S. *J. Phys. Chem. C* **2009**, *113*, 9659.
(52) Medintz, I. L.; Stewart, M. H.; Trammell, S. A.; Susumu, K.; Delehanty, J. B.; Mei, B. C.; Melinger, J. S.; Blanco-Canosa, J. B.; Dawson, P. E.; Mattoussi, H. *Nat. Mater.* **2010**, *9*, 676.
(53) Kovtun, O.; Tomlinson, I. D.; Sakrikar, D. S.; Chang, J. C.; Blakely, R. D.; Rosenthal, S. J. *ACS Chem. Neurosci.* **2011**, *2*, 370.
(54) Cooper, D. R.; Suffern, D.; Carlini, L.; Clarke, S. J.; Parbhoo, R.; Bradforth, S. E.; Nadeau, J. L. *Phys. Chem. Chem. Phys.* **2009**, *11*, 4298.
(55) Hodgkins, J. E.; Ettlinger, M. G. *J. Org. Chem.* **1956**, *21*, 404.
(56) Tajima, H.; Li, G. *Synlett* **1997**, 773.
(57) Li, G.; Tajima, H.; Ohtani, T. *J. Org. Chem.* **1997**, *62*, 4539.
(58) Qu, L. H.; Peng, Z. A.; Peng, X. G. *Nano Lett.* **2001**, *1*, 333.
(59) Clapp, A. R.; Goldman, E. R.; Mattoussi, H. *Nat. Protoc.* **2006**, *1*, 1258.
(60) Mei, B. C.; Susumu, K.; Medintz, I. L.; Mattoussi, H. *Nat. Protoc.* **2009**, *4*, 412.
(61) Mei, B. C.; Susumu, K.; Medintz, I. L.; Delehanty, J. B.; Mountziaris, T. J.; Mattoussi, H. *J. Mater. Chem.* **2008**, *18*, 4949.
(62) Dowgiallo, A. M.; Knappenberger, K. L. *Phys. Chem. Chem. Phys.* **2011**, *13*, 21585.
(63) McArthur, E. A.; Morris-Cohen, A. J.; Knowles, K. E.; Weiss, E. A. *J. Phys. Chem. B* **2010**, *114*, 14514.
(64) Liu, Y. S.; Sun, Y.; Vernier, P. T.; Liang, C. H.; Chong, S. Y.; Gundersen, M. A. *J. Phys. Chem. C* **2007**, *111*, 2872.
(65) Gao, X.; Chan, W. C.; Nie, S. *J. Biomed. Opt.* **2002**, *7*, 532.
(66) Durisic, N.; Godin, A. G.; Walters, D.; Grutter, P.; Wiseman, P. W.; Heyes, C. D. *ACS Nano* **2011**, *5*, 9062.
(67) Sapsford, K. E.; Pons, T.; Medintz, I. L.; Higashiya, S.; Brunel, F. M.; Dawson, P. E.; Mattoussi, H. *J. Phys. Chem. C* **2007**, *111*, 11528.
(68) Laviron, E. *J. Electroanal. Chem.* **1984**, *164*, 213.
(69) Kissinger, P. T.; Heineman, W. R. *J. Chem. Educ.* **1983**, *60*, 702.
(70) Hermanson, G. T. *Bioconjugate Techniques*; Academic Press: San Diego, CA, 1996.
(71) Mattoussi, H.; Palui, G.; Na, H. B. *Adv. Drug Delivery Rev.* **2012**, *64*, 138.
(72) Oh, E.; Susumu, K.; Blanco-Canosa, J. B.; Medintz, I. L.; Dawson, P. E.; Mattoussi, H. *Small* **2010**, *6*, 1273.
(73) Li, Z.; Jin, R.; Mirkin, C. A.; Letsinger, R. L. *Nucleic Acids Res.* **2002**, *30*, 1558.
(74) Maus, L.; Spatz, J. P.; Fiammengo, R. *Langmuir* **2009**, *25*, 7910.
(75) Xia, X.; Yang, M.; Wang, Y.; Zheng, Y.; Li, Q.; Chen, J.; Xia, Y. *ACS Nano* **2012**, *6*, 512.
(76) Iyer, G.; Michalet, X.; Chang, Y.-P.; Pinaud, F. F.; Matyas, S. E.; Payne, G.; Weiss, S. *Nano Lett.* **2008**, *8*, 4618.
(77) Clapp, A. R.; Medintz, I. L.; Mauro, J. M.; Fisher, B. R.; Bawendi, M. G.; Mattoussi, H. *J. Am. Chem. Soc.* **2004**, *126*, 301.
(78) Jana, S.; Maiti, A. K.; Bagh, M. B.; Banerjee, K.; Das, A.; Roy, A.; Chakrabarti, S. *Brain Res.* **2007**, *1139*, 195.
(79) Burda, C.; Green, T. C.; Link, S.; El-Sayed, M. A. *J. Phys. Chem. B* **1999**, *103*, 1783.
(80) Lou, Y. B.; Chen, X. B.; Samia, A. C.; Burda, C. *J. Phys. Chem. B* **2003**, *107*, 12431.
(81) Wang, C. J.; Shim, M.; Guyot-Sionnest, P. *Science* **2001**, *291*, 2390.
(82) Shim, M.; Guyot-Sionnest, P. *Phys. Rev. B* **2001**, *64*, Art. No. 245342.
(83) Kucur, E.; Riegler, J.; Urban, G. A.; Nann, T. *J. Chem. Phys.* **2003**, *119*, 2333.
(84) Kucur, E.; Bucking, W.; Giernoth, R.; Nann, T. *J. Phys. Chem. B* **2005**, *109*, 20355.